IOP Conf. Series: Materials Science and Engineering **263** (2017) 032001 doi:10.1088/1757-899X/263/3/032001

Nontronite mineral identification in nilgiri hills of tamil nadu using hyperspectral remote sensing

M. Vigneshkumar and Kiran Yarakkula
Centre for Disaster Mitigation and Management, Vellore Institute of Technology, Vellore, Tamil Nadu, India – 632014

Email : kiranyadavphysik@gmail.com

Abstract. Hyperspectral Remote sensing is a tool to identify the minerals along with field investigation. Tamil Nadu has abundant minerals like 30% titanium, 52% molybdenum, 59% garnet, 69% dunite, 75% vermiculite and 81% lignite. To enhance the user and industry requirements, mineral extraction is required. To identify the minerals properly, sophisticated tools are required. Hyperspectral remote sensing provides continuous extraction of earth surface information in an accurate manner. Nontronite is an iron-rich mineral mainly available in Nilgiri hills, Tamil Nadu, India. Due to the large number of bands, hyperspectral data require various preprocessing steps such as bad bands removal, destriping, radiance conversion and atmospheric correction. The atmospheric correction is performed using FLAASH method. The spectral data reduction is carried out with minimum noise fraction (MNF) method. The spatial information is reduced using pixel purity index (PPI) with 10000 iterations. The selected end members are compared with spectral libraries like USGS, JPL, and JHU. In the Nontronite mineral gives the probability of 0.85. Finally the classification is accomplished using spectral angle mapper (SAM) method.

1. Introduction

Hyper spectral remote sensing has large number of bands compared to multispectral remote sensing. From the huge amount of spectral information it is applicable into the various application such as agriculture monitoring, pollution, landuse/landcover, soil and water quality monitoring, mineral identification, food quality monitoring and etc [1]. A mineral arises material in nature, signified by a chemical formula, that is often solid and inorganic, and has a crystal arrangement. Out of 5,300 known mineral, 5,070 minerals have been accepted by the International Mineralogical Association (IMA) [2]. The silicate minerals composed more than 90% of Earth's layer. Every minerals have various spectral information depends on its physical and chemical property. Nontronite is the iron (III) wealthy element of the smectite group of clay minerals [3]. Nontronite has a chemical symphony consisting more than 30% Fe_2O_3 and less than 12% Al_2O_3 (ignited basis). It appearances from the weather conditions of biotite and basalts, rainfall of iron and silicon affluent hydrothermal liquids and in bottomless sea hydrothermal vents[4]. Microorganisms are also anxious in reduction of structural iron in nontronite when soils undergo anoxia, and the concentrated form of the clay become visible to be extremely hasty towards certain pollutants, perhaps contributing to the demolition of these compounds in the environment [5]. Figure1 shows the Nontronite mineral and its field spectra. In the present study removal of bad bands, removal of vertical strips in the

images, radiometric calibration, FLAASH atmospheric correction, minimum noise fraction, pixel purity index are performed to process the hyperspectral data. Finally spectral angle mapper (SAM) classification technique approached to classify the hyperion data.

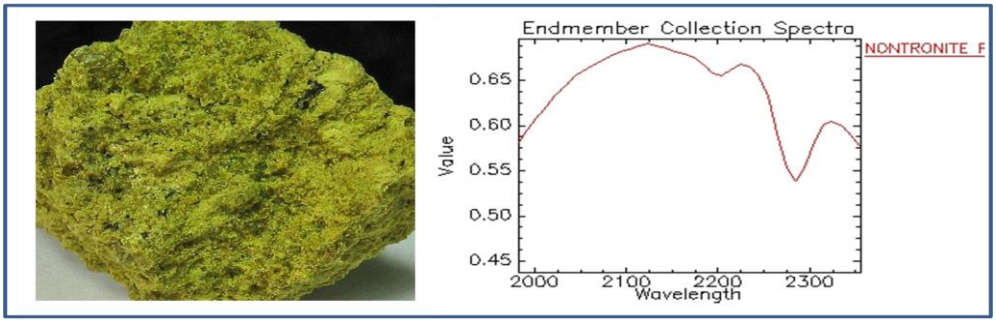

Figure 1. Nontronite mineral and its spectral plot

2. Study area

In Tamil Nadu state government contribute only 2.74% mineral production in overall India. The Nilgiris District of Tamil Nadu lies in the latitude 11° 08' to 11° 37' N and longitude of 76° 27' E to 77° 4' E. Most important metallic and non-metallic mineral presented in Nilgiris district such as iron ore, bauxite and clay utilize in different industries.

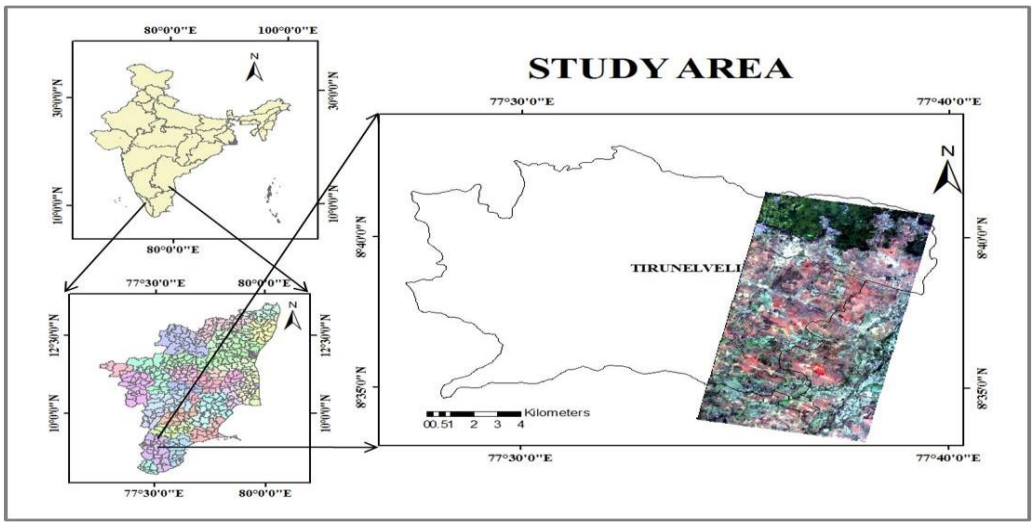

Figure 2. Geological location of the study area

Iron ore take places in the type of Magnetise Quartz in Devala. The iron ore exists in the areas of Illhorai, Kodaperunad, Snowdown, Tellanvedu, Trichagudi, Karudugalai, Masinagudi, Madapad and Adjur of Nilgiris district. The excellence of iron ores presumed about 35 to 38% conserve in every place are about a lakh tonnes. Magnetise, quartz and hematite are crop up in Devala, excellence of series from 35 to 38% and 58% and their reserves are predictable around 11 million tonnes. Bauxite is a hydride of aluminium, take place only close to Kotagiri of Nilgiris district. The fineness of Bauxite availability is 40%. Magnetise is a carbonate of Magnesium enclose 47.6% Magnesia and 52.4% Co_2. The deposit is located at Thengumaranada in Moyar valley. Clay in the constitution of China clay arises in Cherambadi of Nilgiris district. A total set to the side of clay is expected roughly 25,000 tonnes [6].

2.1. Hyperion

In the current study hyperion data is used to recognize the Nontronite mineral. Hyperion is a US satellite has 242 spectral bands in the spectral variety between 0.4 to 2.5 µm at 10nm interval and

calibrate in 16 bit radiometric resolution. The swath-width is 7.2km and the altitude is 705 km. It has 30m spatial resolution and 16 days once revisit period [7]. Hyperion scanner imagery needs proper preprocessing steps like bad bands removal, vertical strips removal, convert the DN values to the radiance value, atmospheric correction like FLAASH, QUAC and etc [8]. Table 1 shows the metadata information of the hyperspectral data. The Visible and VNIR region (0.4-1.2 μm) of hyperion from band 1 to band 70, and is mainly used for vegetation mapping. The SWIR (1.2-2.5μm) of hyperion from band 71 to band 224 [9]. Out of 242, only 198 bands are calibrated due to not illuminated and sensor overlap problem [10]. Figure 2 shows the geological location of the study area.

Table 1. Metafile information of downloaded Hyperion data

Data Set Attribute	**Attribute Value**
Entity ID	EO1H144052201606311
Acquisition Date	3/3/2016
Cloud Cover	0 to 9%
Scene Start Time	2016:063:03:15:24.581
Scene Stop Time	2016:063:03:15:39.581
Sun Angle	29.87^0
Satellite Inclination	97.97^0
Look Angle	-18.493
Center area Latitude, Longitude	11°11'50.00"N, 76°29'21.78"E
NW Corner Latitude, Longitude	12°03'54.26"N, 76°35'22.25"E
NE Corner Latitude, Longitude	12°03'01.25"N, 76°39'51.08"E
SE Corner Latitude, Longitude	11°11'50.00"N, 76°29'21.78"E
SW Corner Latitude, Longitude	11°12'43.03"N, 76°24'53.76"E

3. Methodology

To classify the hyperspectral data, various preprocessing steps are required. Figure 3 explains the through methodology involved to process the hyperion data.

3.1. Remove the zero bands and bad bands

Hyperion imagery contains pixels without information called as zero bands. They are present in 1-7, 58-76, 225-242 bands [11]. Bad bands contain lots of noise and water vapor in the spectral region. It may varies for every image depends on the location and scanning time [12].

3.2. Remove the vertical stripe in the imagery

In push-broom scanner, number of vertical strips is present in the column. The raw image has several dark and bright columns happening due to change in the calibration or failure of some detectors in the CCD display at the moment of imprison the image. Examine column dropout or band errors should be removed before atmospheric corrections [13]. The dreadful columns are replaced by taking average of the previous and next column [13]. In the present study local destriping algorithm is used to remove the strips.

$$\sum_{j=1}^{n} \frac{(x_{i-1,j,k})+(x_{i+1,j,k})}{2n} \qquad (1)$$

The equation 1 shows the local destriping algorithm.

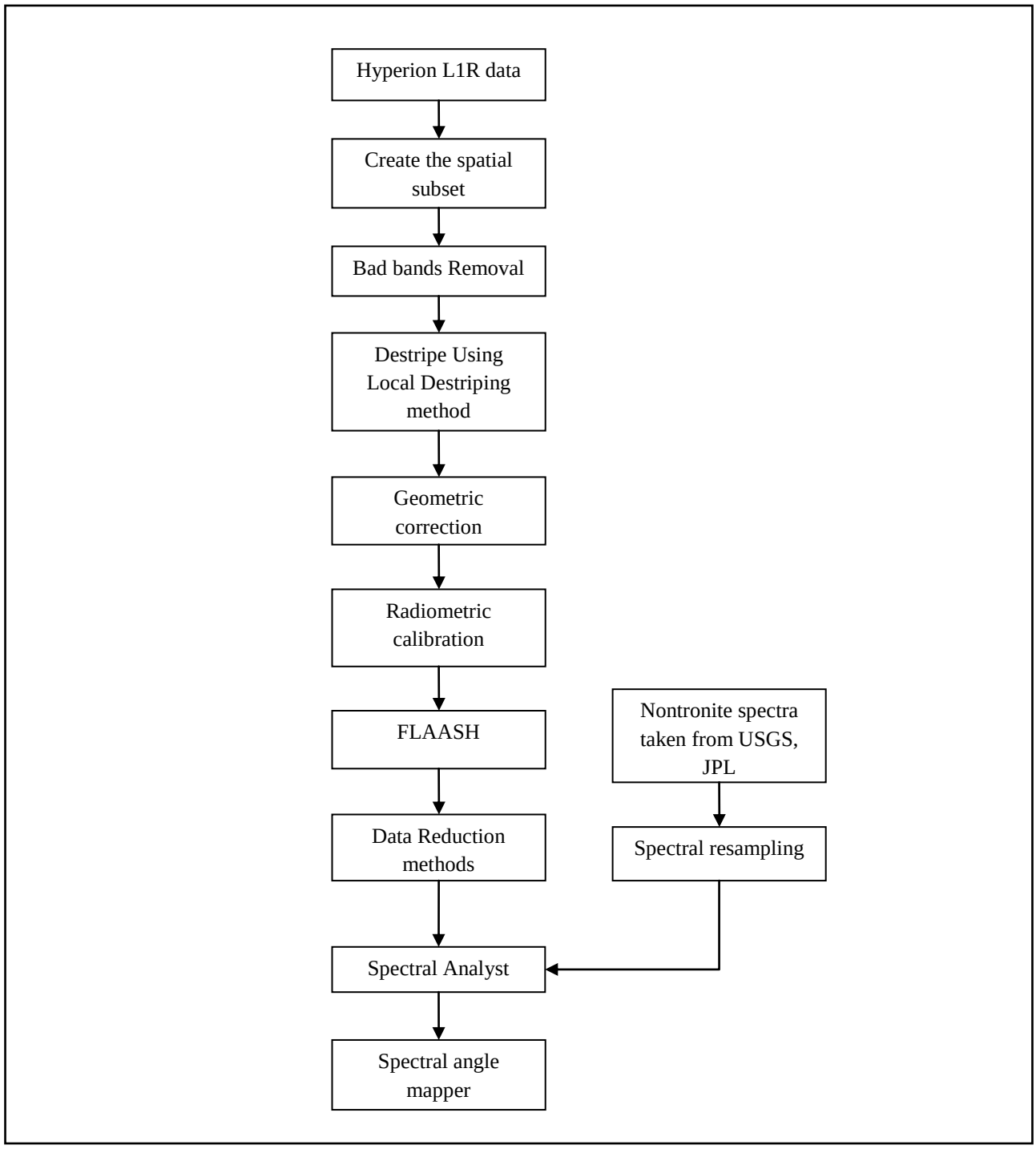

Figure 3. Methodology of the research work

3.3. Radiometric calibration

Radiance is the amount of light energy detected by the instrument from the object being observed [14]. Radiometric calibration applied during remote sensing data dispensation and contains corrections associated to the sensitivity of the remote sensor, topography and sun angle, and atmospheric scattering and absorption. It is mainly familiar with convert the digital numeral to radiance value in favor of each pixel. It has three types of formats BSQ, BIP and BIL [15].

3.4. Fast Line-of-sight Atmospheric Analysis of Hypercube (FLAASH)
FLAASH corrects the wavelengths in VNIR and SWIR region up to 3 μm. FLAASH comprises the following features such as correction for the adjacency consequence, to compute a scene-average visibility, cirrus and opaque cloud map and Modifiable spectral shineing for artifact repression [16].

3.5. Minimum noise fraction (MNF)
MNF is mostly employed to decrease the dimensionality of hyperspectral data and developed as an option to principle component analysis. It is distinct as a two-pace cascaded PCA. The first pace, based on probable noise covariance matrix, is to decorrelate and rescale the data noise, it has item discrepancy and no band-to-band correlations. The second pace is a typical PCA of the noise-whitened data [17]. It partitions the data space into two segments, one related with big Eigen values and rational Eigen images, and a second with near to unity Eigen values and noise-conquered images. By means of only the rational segments in succeeding processing, the noise is divided from the data, thus humanizing spectral processing consequences [18].

3.6. Pixel Purity index (PPI)
The pixel purity index algorithm is manipulated for every pixel in the image cube by arbitrarily generate appearance in the N-dimensional, a distribute scheme of the MNF transformed information [19]. Total points in the space are now predictable into the lines and those ones that go down at the extremes of the lines are calculated. After numerous projections to dissimilar lines, individual pixels that count above a assured threshold are stated "pure" [20].

3.7. Spectral analysis
Spectral analysis assists to classify materials based on their spectral distinctiveness. The spectral analysis uses various methods for instance binary encoding, spectral angle mapper, and spectral feature fitting to rank the equivalent of an image spectrum to the minerals available in a spectral library [21].

3.8. Spectral angle mapper
SAM computes the angular distance between reflection spectrum in the image and the mineral spectra in n -dimensions. The classified image shows the most excellent SAM match at each pixel for every end member viewing the angular distance in radians between image spectrum and reference spectrum. Darker pixels symbolize lesser spectral angles, and the spectra parallel to the reference spectrum. The rule images can be employed for categorizations using various thresholds to choose the pixels are incorporated in the SAM image [22].

4. Results and Discussion

4.1. Removing the bad bands from hyperion data
Hyperion data has a total of 242 bands, out of which 163 bands in calibrating condition, other bands are affect by noise, non-illuminated and water vapor [23]. Table 2 shows the list of unused and bad bands in the hyperion sensor. Figure 4 clearly shows the zero bands, overlap region. Figure 5 shows the spectral profile plot after removing the zero bands and overlap region. Figure 4 and 5 shows the effect of bad bands removing in the spectral profile plot

Table 2. List of unused bands in hyperion sensor

S.No	Bad bands	Reason
1	1-7	Zero bands, Non-illuminated
2	58-76	Zero bands, Overlap region between VNIR-SWIR region
3	121-132	Water vapor region has lot of Noise
5	165-181	Water vapor region has lot of Noise
6	221-224	Water vapor region has lot of Noise
7	225-242	Zero bands, Non-illuminated

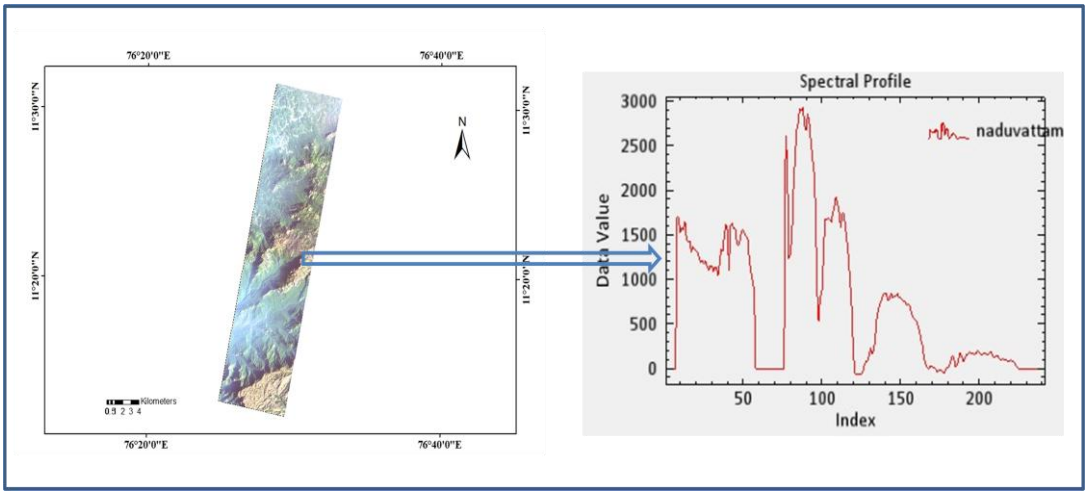

Figure 4. Before removing the bad bands and its spectral plot

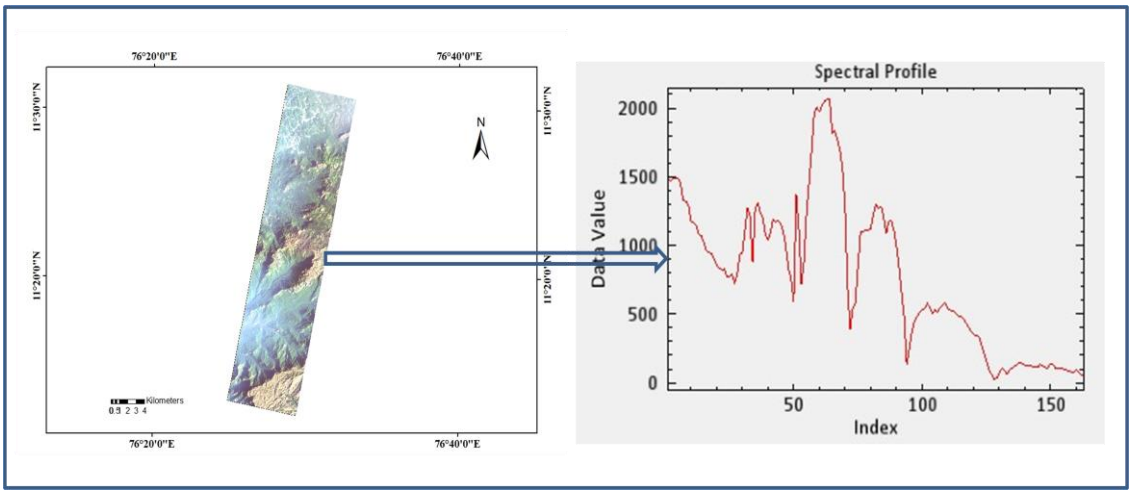

Figure 5. After removing the bad bands and its spectral plot

4.2 Destriping

The vertical strips are removed using local destriping approaches. They are highly recommended for vertical stripe removal, because it modify strip column layer only [24]. The vertical strips removed process improve the correlation between the reflection spectra and mineral spectra and helps to formulate precision in mineral classification [25]. Table 3 shows the vertical strips availability in the imagery column. Figure 6 shows the spectral profile plot and visualization variation after removing the vertical strips.

Table 3. List of vertical strips in hyperion imagery

S. No	Bands	Column	S. No	Bands	Column
1	8,9	6, 68, 114	8	135	60
2	10,11	6,114,199	9	158	18
3	87	54	10	162	103
4	94	92	11	198	117
5	99	91	12	202	182
6	116	137	13	201	7
7	118	145	14	203	114

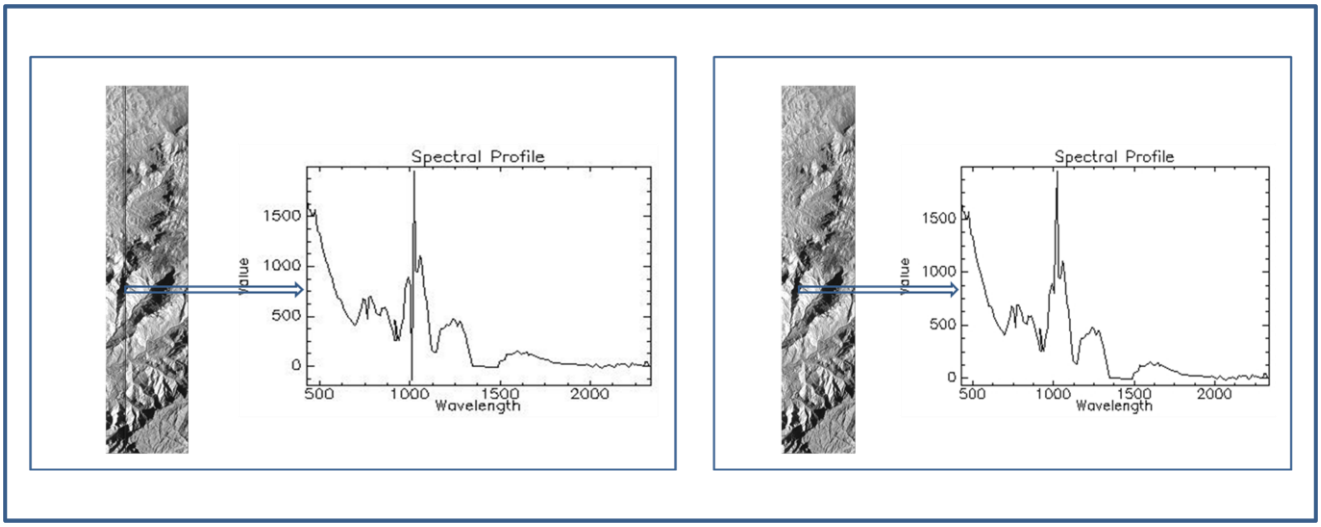

Figure 6. Effect of destriping in visual interpretation and its spectral plot

4.3. Radiometric calibration

The radiometric calibration uses to get the radiance value of the earth surface from the DN value of hyperion data. The scale factor applies 0.1 and the output file format is given as BIL (Band Interleaved by Pixel). It converts the hyperion CCD digital numbers to radiance value [26]. Figure 7 shows the radiance value and its spectral profile plot.

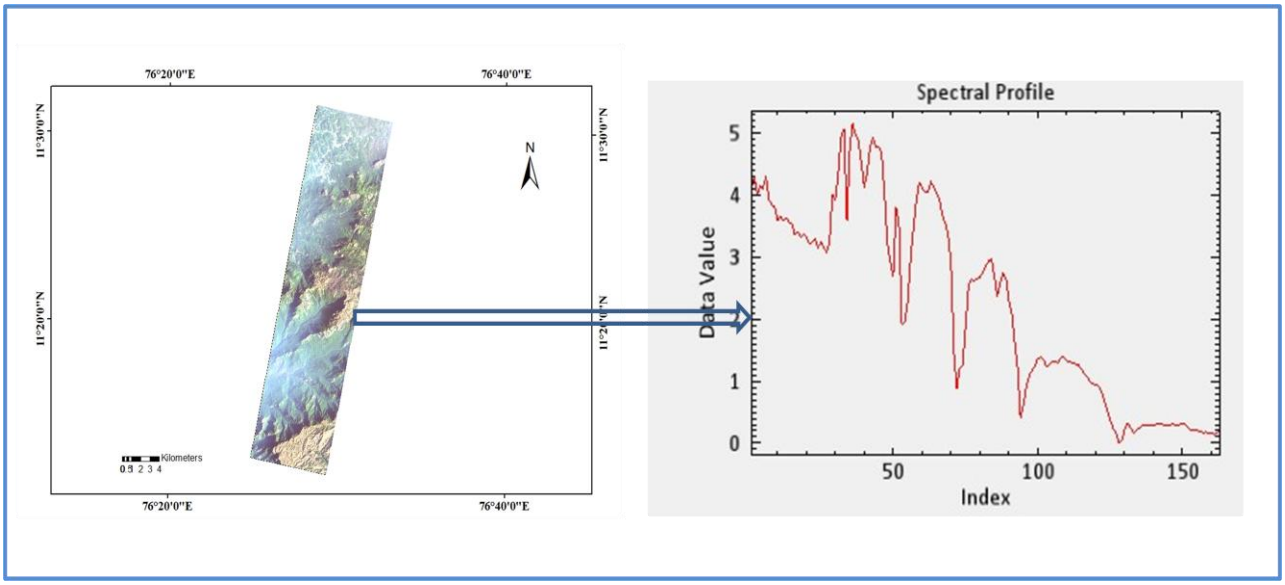

Figure 7. Radiometric calibration and its spectral plot

4.4. Atmospheric correction module

Atmospheric correction module is performed using FLAASH module. FLAASH uses the superior techniques to handle mainly stressing atmospheric conditions, such as the attendance of clouds. The input image for FLAASH is radiometric calibrated radiance image in BIL format. The data is 4-byte signed numerals [27]. Figure 8 shows the reflectance value and its spectral profile plot using FLAASH module.

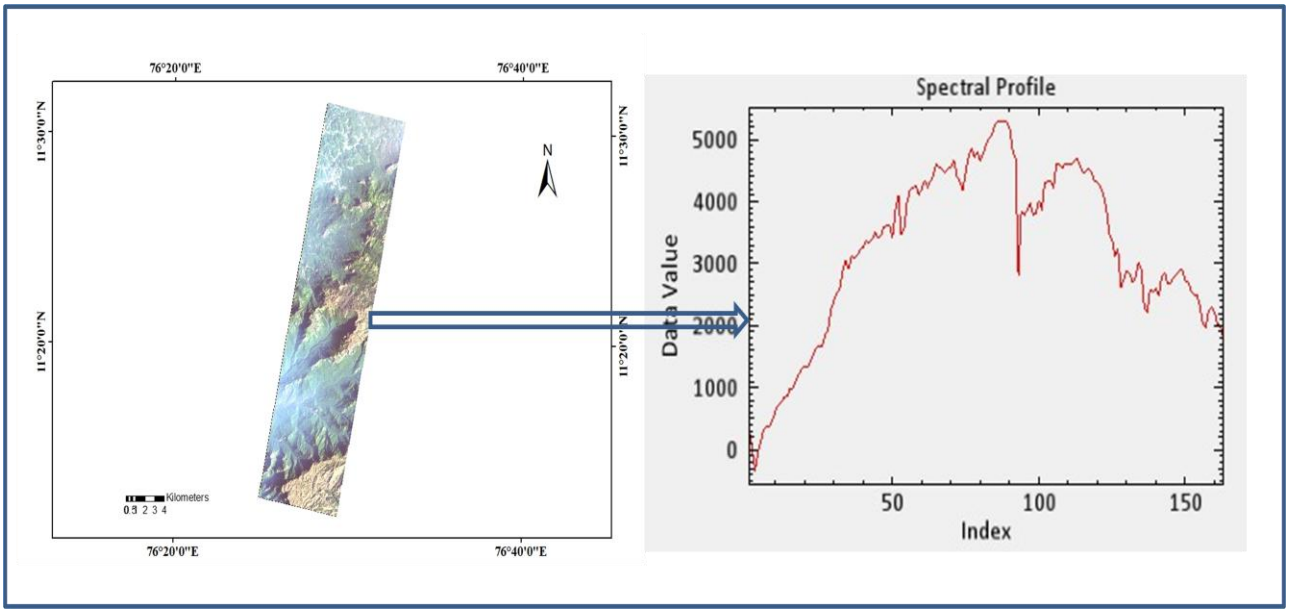

Figure 8. FLAASH module and its spectral plot

4.5. Minimum Noise Fraction (MNF)

The reflectance bands of hyperion imagery contains lot of noise information. The MNF transformation is the advance method of PCA. MNF sorts the reflectance bands in the ascending order depends the noise availability [28]. Figure 9 clearly shows the large amount of noise present in the data and it affect the descending order bands. MNF takes only 9 bands in the region to process the hyperion data.

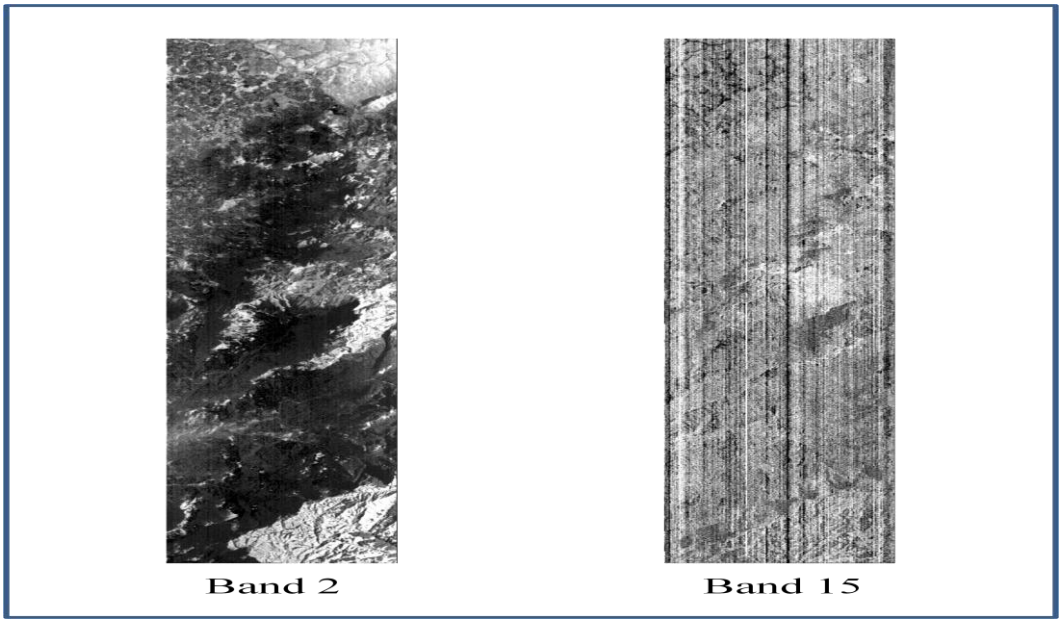

Figure 9. MNF sorting the bands depends on the noise level

4.6. Pixel Purity Index (PPI)

The noiseless bands generated from MNG given as input for pixel purity index. PPI process the MNF bands in the threshold limit of 2.5 to 10000 iterations. The black and white pixels in the PPI represent impure and pure pixels respectively [29]. Figure 10 represents pixel purity index image.

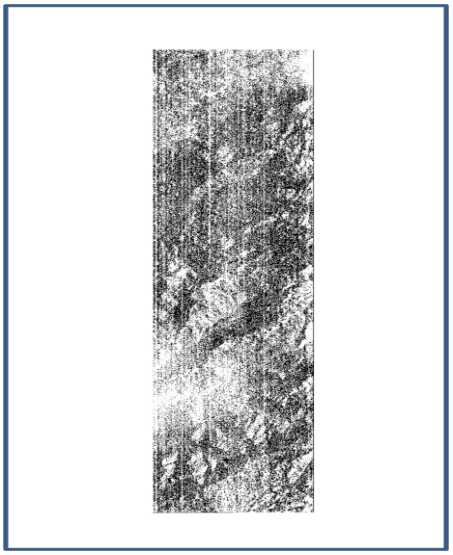

Figure 10. Pixel purity index

4.7. Spectral Analysis

The Nontronite mineral spectra is taken from the spectral libraries like USGS, JPL, JHU [22]. The band interval of this mineral spectra is 2.5nm but the hyperion imagery spectra interval is 10nm. Spectral Resembling methods implements to convert the library spectra information from 2.5nm to 10nm intervals [30]. The spectral analyst tool compares the nontronite mineral spectra to image spectra and gives probability using the methods such as SAM, SFF, BE. In this research work Nontronite mineral gives high probability around 0.85 in the wavelength region between 2000nm - 2500nm.

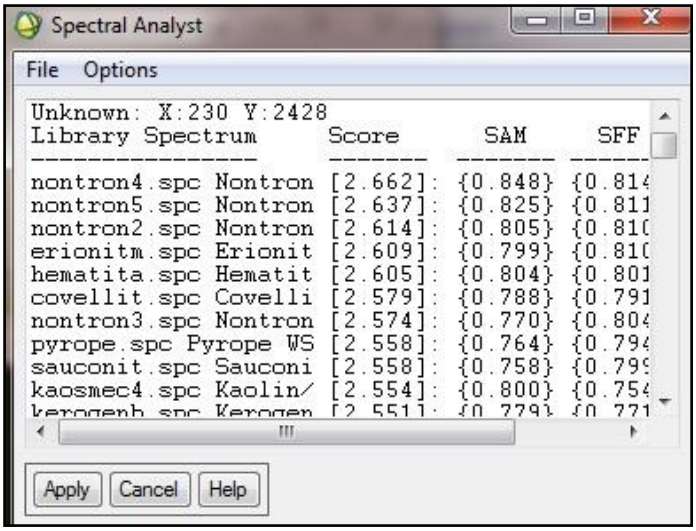

Figure 11. Nontronite mineral probability

Figure 11 shows the overall probability score obtain compares the image spectra with mineral spectra. Figure 12 shows the correlation between the image spectra and mineral spectra. The white line indicates the mineral spectra. The red line indicated the image spectra.

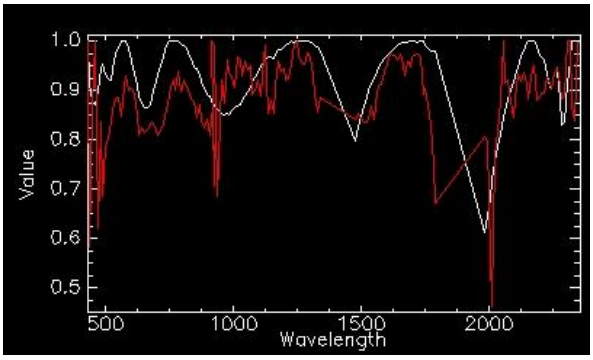

Figure 12. Correlation between the image spectra and library spectra

4.8. Spectral Angle Mapper

In the spectral angle mapper method compares the image spectrum and Nontronite spectra. The band selection taken from 1900nm to 2400nm in SWIR region [31]. The angle variation between the image spectra and mineral spectra given as 0.25. SAM result produces the red pixels indicate the Nontronite mineral in the earth terrain. Figure 13 shows the Nontronite mineral classifed using SAM. The black pixels indicate the other earth surface things occupied in the region. In Nilgiris contain lot of vegetation and tree surfaces, they are affect the mineral reflectance.

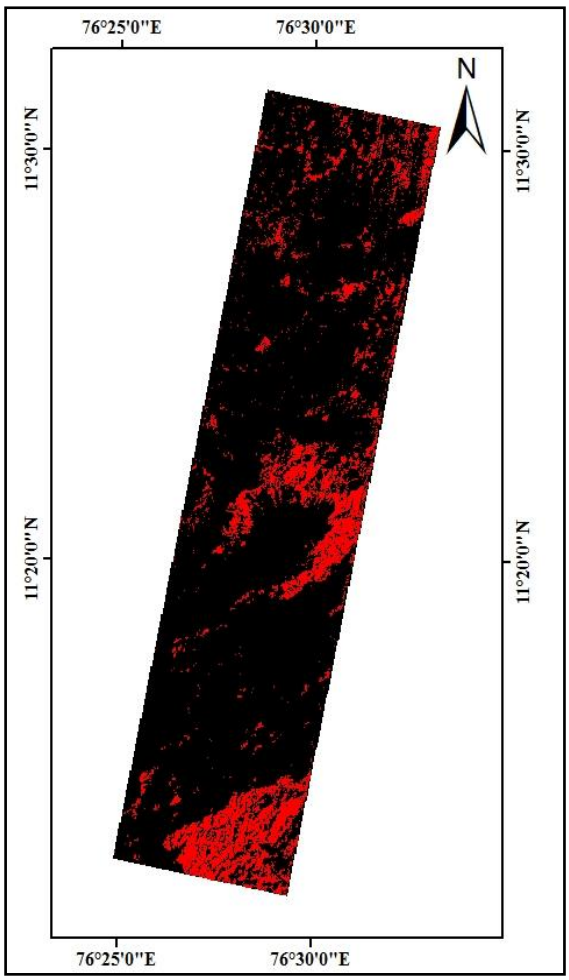

Figure 13. Spectral angle mapper - Nontronite mineral identification result

5. Conclusion

In hyperion imagery out of 242, 142 bands available in the calibration condition. The vertical strips are removed using local destriping algorithm. The absolute reflectance of the area carried out using FLAASH module. The spectral information reducing using the minimum noise fraction techniques only 8 reflection bands are taken. Apply the noiseless bands to the pixel purity index and purest pixels of the earth surfaces are taken. The spectral analyst compares the image spectra and mineral spectra, its produce the probability around 8.48 and overall score around 2.662. Finally the spectral angle mapper produce the Nontronite mineral mapping in the angle variation of 0.25.

References

[1] Zhang L and Du B 2012 Recent advances in hyperspectral image processing *Geo-spatial Inf. Sci.* **15** 143–56

[2] Schneider S, Murphy R J and Melkumyan A 2014 Evaluating the performance of a new classifier – the GP-OAD: A comparison with existing methods for classifying rock type and mineralogy from hyperspectral imagery *ISPRS J. Photogramm. Remote Sens.* **98** 145–56

[3] Kumari S K, Debashish C, Pulakesh D and Jatisankar B 2014 Hyperion Image Analysis for Iron Ore Mapping in Gua Iron Ore Region , *Int. Res. J. Earth Sci.* **2** 1–6

[4] E S L and Yarrakula K 2017 Comparative analysis of digital elevation models : A case study around Madduleru River **46** 1339–51

[5] Lin L, Wang Y, Teng J and Wang X 2016 Hyperspectral analysis of soil organic matter in coal mining regions using wavelets , correlations , and partial least squares regression

[6] Ahlawat V, Jhorar O, Kumar L and Backhouse D 2011 Using hyperspectral remote sensing as a tool for early detection of leaf rust in blueberries *34th Int. Symp. Remote Sens. Environ.* 2–5

[7] Tuominen J, Lipping T, Kuosmanen V and Haapanen R 2009 Remote Sensing of Forest Health *Geosci. Remote Sens.* 29–52

[8] Magendran T 2009 Hyperspectral radiometry to estimate the grades of iron ores of Naomundi, India

[9] Upadhyay R 2012 Mineral abundance mapping using hyperion dataset in Udaipur , India *14th Annual International Conferance and Exhibition on Geospatial - Information Technology* pp 1–8

[10] Ganesh B P, Aravindan S, Raja S and Thirunavukkarasu a. 2012 Hyperspectral satellite data (Hyperion) preprocessing—a case study on banded magnetite quartzite in Godumalai Hill, Salem, Tamil Nadu, India *Arab. J. Geosci.* 3249–56

[11] Zeng W-Z, Huang J-S, Xu C, Ma T and Wu J-W 2016 Hyperspectral reflectance models for soil salt content by filtering methods and waveband selection *Ecol. Chem. Eng. S* **23** 117–30

[12] Peppin W A and Beddell R L 2009 Hyperspectral image classification for mineralogical identification

[13] Pal and Porwal 2015 Destriping of Hyperion Images Using Low-Pass- Filter and Local-Brightness-Normalization *IGARSS 2004. 2004 IEEE Int. Geosci. Remote Sens. Symp.* 3509–12

[14] Arellano P, Tansey K, Balzter H and Boyd D S 2015 Detecting the effects of hydrocarbon pollution in the Amazon forest using hyperspectral satellite images. *Environ. Pollut.* **205** 225–39

[15] Srivastava R, Sarkar D, Mukhopadhayay S S, Sood A, Singh M, Nasre R A and Dhale S A 2015 Development of hyperspectral model for rapid monitoring of soil organic carbon under precision farming in the Indo-Gangetic Plains of Punjab, India *J. Indian Soc. Remote Sens.* **43** 751–9

[16] Kumar C, Shetty A, Raval S, Sharma R and Ray P K C 2015 Lithological Discrimination and Mapping using ASTER SWIR Data in the Udaipur area of Rajasthan, India *Procedia Earth Planet. Sci.* **11** 180–8

[17] Sahoo S R, Panda P K, Ray P K C and Division G 2015 HYPERSPECTRAL IMAGE ANALYSIS FOR IRON ORE DISCRIMINATION IN KEONJHAR DISTRICT , ODISHA

Data Pre-Processing *Int. J. Remote Sens. Geosci.* **4** 28–34
[18] Crosta A 2015 Hyperspectral remote sensing for mineral mapping : a case-study at alto Paraíso de Goías , central Brazil *J. Geosci.* **30**
[19] Ramakrishnan D and Bharti R 2015 Hyperspectral remote sensing and geological applications *Curr. Sci.* **108** 879–91
[20] Sahoo, R. N., S. S. Ray and K R M 2015 Hyperspectral remote sensing of agriculture *Curr. Sci.* **108** 848
[21] Kruse F A, Bedell R L, Taranik J V, Peppin W A, Weatherbee O and Calvin W M 2011 Mapping alteration minerals at prospect, outcrop and drill core scales using imaging spectrometry *Int. J. Remote Sens.* **33** 1780–98
[22] Pour a B and Hashim M 2014 Alteration mineral mapping using ETM+ and hyperion remote sensing data at Bau Gold Field, Sarawak, Malaysia *IOP Conf. Ser. Earth Environ. Sci.* **18** 12149
[23] Scheffler D and Karrasch P 2013 Preprocessing of hyperspectral images: a comparative study of destriping algorithms for EO1-Hyperion *Proc. SPIE Vol. 8892, Image Signal Process. Remote Sens. XIX* **8892**88920H–1–88920H–15
[24] Tsai F, Lin S, Rau J, Chen L and Liu G 2003 Destriping Hyperion Imagery Using Spline Interpolation *Res. gate*
[25] Beiranvand Pour A and Hashim M 2014 ASTER, ALI and Hyperion sensors data for lithological mapping and ore minerals exploration *Springerplus* **3** 130
[26] Zhang C 2014 Combining Hyperspectral and Lidar Data for Vegetation Mapping in the Florida Everglades *Photogramm. Eng. Remote Sens.* **80** 733–43
[27] Kumar M V and Yarrakula K 2017 Comparison of efficient techniques of hyper-spectral image preprocessing for mineralogy and vegetation studies *Indian J. geomarine Sci.* **46** 1008–21
[28] Kempeneers P, Deronde B, Bertels L, Debruyn W, Backer S De and Scheunders P 2004 Classifying hyperspectral airborne imagery for vegetation survey along coastlines *IGARSS 2004. 2004 IEEE Int. Geosci. Remote Sens. Symp.* **2**
[29] Panda S, Banerjee K, Jain M K, Jeyaseelan A T and Sharma R K 2014 Mapping of Iron Minings of Noamundi Areas , Jharkhand By Using the Image Based Ndii and Geospatial Technology *Int. J. Innov. Sci. Res.* **7** 5–10
[30] Das B S, Sarathjith M C, Santra P, Sahoo R N, Srivastava R, Routray A and Ray S S 2015 Hyperspectral remote sensing: Opportunities, status and challenges for rapid soil assessment in India *Curr. Sci.* **108** 860–8
[31] Guha A, Kumar K V, Rao E N D and Parveen R 2014 An image processing approach for converging ASTER-derived spectral maps for mapping Kolhan limestone, Jharkhand, India *Curr. Sci.* **106** 40–9